

Crystal structure of human glycine receptor- α 3 bound to antagonist strychnine

Xin Huang¹, Hao Chen², Klaus Michelsen¹, Stephen Schneider³ & Paul L. Shaffer¹

Neurotransmitter-gated ion channels of the Cys-loop receptor family are essential mediators of fast neurotransmission throughout the nervous system and are implicated in many neurological disorders. Available X-ray structures of prokaryotic and eukaryotic Cys-loop receptors provide tremendous insights into the binding of agonists, the subsequent opening of the ion channel, and the mechanism of channel activation^{1–8}. Yet the mechanism of inactivation by antagonists remains unknown. Here we present a 3.0 Å X-ray structure of the human glycine receptor- α 3 homopentamer in complex with a high affinity, high-specificity antagonist, strychnine. Our structure allows us to explore in detail the molecular recognition of antagonists. Comparisons with previous structures reveal a mechanism for antagonist-induced inactivation of Cys-loop receptors, involving an expansion of the orthosteric binding site in the extracellular domain that is coupled to closure of the ion pore in the transmembrane domain.

Human glycine receptors (GlyRs) are pentameric ligand-gated ion channels (pLGICs) that mediate fast inhibitory synaptic transmission in the spinal cord and brainstem^{9,10}. GlyRs play a key role in motor coordination and the processing of inflammatory pain¹¹. Disruption of the normal function of GlyRs causes hyperekplexia¹², a rare neurological disorder characterized by an exaggerated startle response. GlyRs belong to the large family of Cys-loop receptors, which includes inhibitory anion-selective type A γ -aminobutyric acid receptors (GABA_ARs) together with GlyRs, excitatory cation-selective nicotinic acetylcholine receptors (nAChRs), and serotonin type 3 receptors (5HT₃Rs)¹³. *In vivo*, GlyRs can exist as homopentamers containing only α -subunits or heteropentamers comprising both α - and β -subunits¹⁴. Upon binding of the neurotransmitter glycine to the extracellular domain (ECD), GlyRs undergo conformational changes that allow the transmembrane domain (TMD) to selectively open to permeant anions such as chloride.

X-ray structures of the soluble acetylcholine-binding protein (AChBP), a homologue of the ECD of nAChR, clearly show that the orthosteric binding site is at the subunit interfaces and provide great insight into the binding modes of many agonists and antagonists^{15–18}. Crystal structures of two bacterial pLGIC homologues (ELIC and GLIC)^{1–4} and several eukaryotic pLGICs^{5–8} have recently been solved. The structures of apo^{–8} and agonist-bound⁵ (in closed and open conformations respectively) *Caenorhabditis elegans* glutamate-gated chloride channel (GluCl), the agonist-bound human GABA_AR⁶, the nanobody-bound mouse 5HT3R⁷, and the chimaeric GLIC(ECD)-GlyR α 1(TMD)¹⁹, reveal conformational transitions during activation. Nevertheless, no structural information is available to understand the inactivation mechanism by competitive antagonists. To address this unknown, we solved the crystal structure of a human GlyR, which is a homopentamer of α 3-subunits (GlyR α 3) in complex with strychnine. Strychnine is an alkaloid from poisonous plants that causes muscle spasms, convulsions, and eventual death, and remains in use as a rodenticide. Strychnine exerts its lethal effects by antagonizing GlyRs in the central nervous system^{10,20,21}.

To facilitate the formation of well-ordered crystals, we replaced the 76-residue intracellular loop between the transmembrane helix 3 (M3) and helix 4 (M4) with an Ala-Gly-Thr tripeptide and deleted four residues from the carboxy (C) terminus. When solubilized in detergent, GlyR α 3_{cryst} retained the ability to bind strychnine. Surface plasmon resonance (SPR) and isothermal titration calorimetry (ITC) binding studies indicated that GlyR α 3_{cryst} binds to strychnine with a dissociation constant (K_d) of \sim 50 nM, and ITC studies suggested a stoichiometry of five strychnine molecules per GlyR α 3_{cryst} pentamer (Extended Data Fig. 1a, b), in good agreement with published values for the wild-type GlyR α 3 (ref. 22). Furthermore, HEK293T cells expressing GlyR α 3_{cryst} displayed glycine-dependent conductance of chloride (Extended Data Fig. 2).

We determined the X-ray structure of GlyR α 3_{cryst} in complex with strychnine at 3.0 Å resolution (Fig. 1, Extended Data Fig. 3 and Extended Data Table 1). Similar to the structures of other pLGICs reported previously, GlyR α 3 adopts a cylindrical assembly with a five-fold symmetry and the ion permeation pathway located at the symmetry axis. The ECD comprises an amino (N)-terminal α -helix (α 1) followed by a curled β -sandwich with ten β -strands with a second α -helix (α 2) between β -strands 3 and 4. Four α -helices (M1–4) after the ECD constitute the TMD, with the 20 helices from the five subunits forming a channel and the five M2 helices lining the channel pore. We observed one glycosylation site, Asn38, and at least one sugar moiety on each subunit. These glycans are solvent exposed and do not interact with other residues, unlike the glycans in the GABA_AR structure⁶.

Strychnine is a very potent and selective antagonist of GlyRs, and binds GlyRs competitively with agonists such as glycine^{10,20,21}. In the co-crystal structure, strychnine binds in a pocket at the interface between adjacent subunits, corresponding to the orthosteric binding site of neurotransmitter agonists in other pLGIC structures (Fig. 2 and Extended Data Fig. 4). The strychnine binding pocket is formed by two loops from the principal or (+) subunit, loop C between strands β 9 and β 10 and loop B between strands β 7 and β 8, and β -strands from the complementary or (–) subunit, β 1, β 2, β 5, and β 6. Two Phe residues (63 and 159) form the hydrophobic ‘base’ of the binding pocket for rings V, VI, and VII of strychnine. The ‘flap’ of the binding pocket is composed of residues Tyr202, Thr204, and Phe207 from loop C. Additionally, the backbone carbonyl of Phe159 makes a hydrogen bond with the tertiary amine of strychnine, which is largely protonated at physiological pH ($pK_a = 8.26$). The lactam oxygen is stabilized by the electropositive character of this region of the binding site, in part because of Arg65 (Extended Data Fig. 2f). This binding mode of strychnine in the ‘baseball cap’ shape observed in the co-crystal structure agrees very well with previously published structure–activity relationships of strychnine analogues with GlyRs, which identified the lactam group and the C(21)=C(22) bond as the essential structural features required for strong antagonistic activity towards GlyR α 1 and GlyR α 1 β ^{23,24}.

The importance of the binding-site residues for strychnine is supported by published mutagenesis data^{25–28}. Mutation of Phe63 to alanine results in over 250-fold loss of affinity and mutation of Phe207 to

¹Department of Molecular Structure and Characterization, Amgen Inc., 360 Binney Street, Cambridge, Massachusetts 02142, USA. ²Department of Protein Technologies, Amgen Inc., 360 Binney Street, Cambridge, Massachusetts 02142, USA. ³Department of Neuroscience, Amgen Inc., 360 Binney Street, Cambridge, Massachusetts 02142, USA.

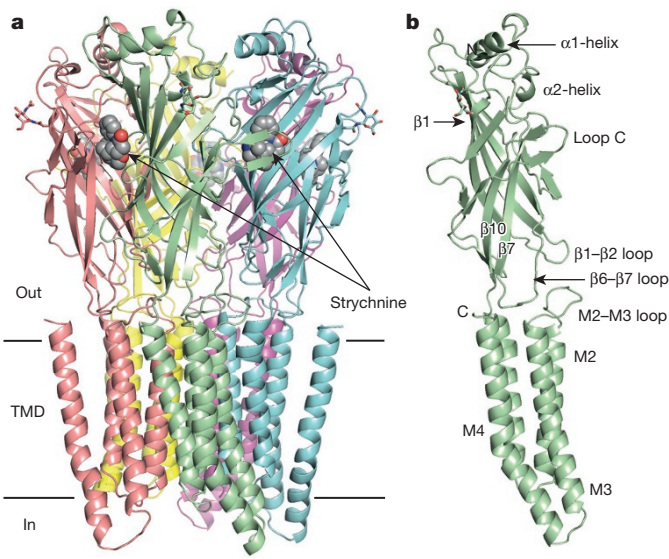


Figure 1 | Architecture of the GlyR α 3 bound to strychnine. **a**, The GlyR α 3-strychnine complex viewed parallel to the plasma membrane. Each subunit is coloured separately. Strychnine is shown as spheres with carbon atoms in grey, nitrogen in blue, and oxygen in red. N-linked glycans are shown as sticks coloured by subunit. **b**, A single subunit of the GlyR α 3 viewed parallel to the membrane but rotated 40° relative to orientation in **a**. Secondary structure elements and important loops are noted.

alanine abolishes strychnine binding. A mutation in rat GlyR α 2 that is equivalent to Gly160Glu in human GlyR α 3 yields striking strychnine insensitivity. In the co-crystal structure, Gly160 C α is in van der Waals contact with the indole ring of strychnine, and addition of the glutamate side chain would prevent strychnine binding in the observed orientation. While the residues critical for strychnine binding are identical among the α - and β -subunits of GlyRs (except that the residue corresponding to Phe207 is a conservatively substituted Tyr in the β -subunit), some of them are not conserved in other pLGICs such as nAChR and 5-HT3R (Extended Data Fig. 5). This explains why strychnine is a competitive antagonist specific to GlyRs.

Superposition of the strychnine-binding site in our co-crystal structure with the agonist-binding sites in the structures of other pLGICs revealed one clear difference (Extended Data Fig. 6). The orthosteric binding site is larger and loop C adopts an open conformation in the strychnine-bound state, reminiscent of antagonist-bound AChBP structures¹⁷. In contrast, the orthosteric site is smaller and loop C adopts a closed conformation in the agonist-bound state of GluCl⁵ and GABA_AR⁶, capping the binding site.

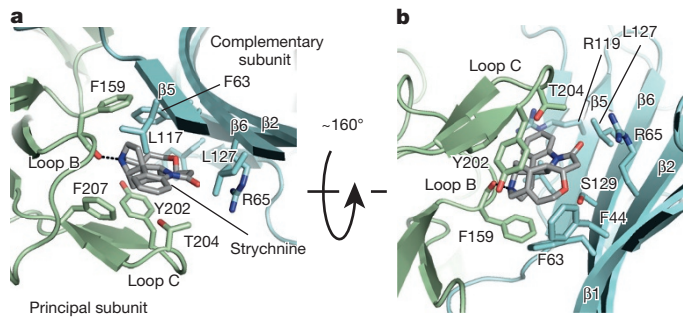
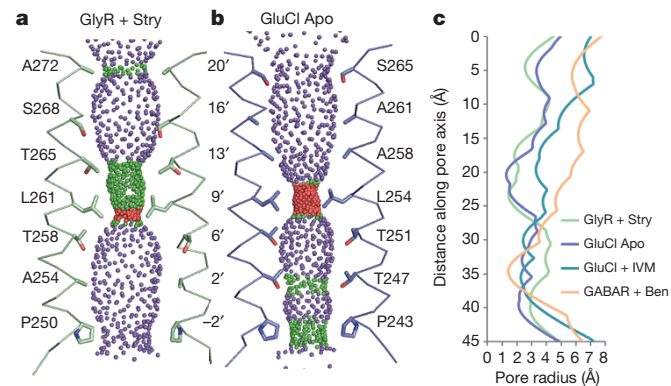


Figure 2 | Orthosteric binding site occupied by the antagonist strychnine. **a**, Two views of the strychnine-binding site. The view in **a** is from above the receptor looking down, perpendicular to the plasma membrane. Strychnine is shown as grey sticks. The principal subunit is coloured in pale green and the complementary subunit is coloured in cyan. Important residues and secondary structure elements are noted. Black dashed line indicates hydrogen bond from the backbone carbonyl oxygen of Phe159 to the tertiary amine of strychnine.

The ion channel pore of GlyR α 3 is lined by the transmembrane helix M2. There are several constrictions along the length of the GlyR α 3 pore, down to the narrowest 1.4 Å caused by the side chain of Leu261 (Leu 9') in the mid-point of the channel. Since the radius of a dehydrated chloride ion is 1.8 Å, the ion channel of strychnine-bound GlyR α 3 is consistent with a closed, non-conducting state. Leu261 (Leu9') thus forms the shut gate of the ion channel. Leu261 is highly conserved and mutation of the equivalent Leu285 in GlyR β to Arg has been linked to hyperekplexia (Extended Data Fig. 5)¹². Another highly conserved residue Pro250 (Pro-2') of M2 occupies the cytoplasmic end of the ion channel. Pro250 is critical for ion selectivity and mutation Pro250Thr in GlyR α 1 has been linked to hyperekplexia¹². Other hyperekplexia mutations in GlyR α 1 (V260M, T265I, Q266H, and S267N) with spontaneous channel activity¹² are also clustered on the pore-lining M2 helix. In the antagonized state of GlyR α 3, all five M2 helices are straight and oriented parallel to the pore axis (Fig. 3a). In contrast, in the apo structure of GluCl⁸ and the agonist-bound structures of GluCl⁵ and GABA_AR⁶, the M2 helices tilt outwards at the pore apex (Fig. 3b, c). The GlyR α 3-strychnine M2 helices are 11.0 Å apart at the apex (Ala272), 11.7 Å at the base, and 13.0 Å at the most constricted point (Leu261), averaging the distance between C α carbons of *i* and *i* + 2 protein subunits. In comparison, the apo-GluCl pore is 12.6 Å at the apex (Ser265), 10.3 Å at the base (Pro243), and 12.5 Å at the most constricted point (Leu254). This corresponds to an ~4° tilt of the M2 helix towards the pore axis in the strychnine-bound state (Fig. 4a)⁸. Transition from the apo- to the agonist-bound state of GluCl involves tilting of M2 helix by ~8° away from the pore axis, which relieves the occlusion of the pore by Leu254 (ref. 5).

For an agonist- or antagonist-binding event to affect the state of the channel, the signal must be transduced across the ECD-TMD interface. Besides the covalent connection by the β 10-M1 linker, the ECD-TMD interface of GlyR α 3 also contains hydrophobic contacts between the N-terminal portion of the M2-M3 loop, the β 1- β 2 loop, and the β 6- β 7 ('Cys') loop as well as polar contacts between the C-terminal portion of the M2-M3 loop and the β 6- β 7 loop (Fig. 4b and Extended Data Fig. 7). Pro275 (from the M2-M3 loop) interacts with Leu142 and Phe145 (from the β 6- β 7 loop) through their side chains and the side-chain hydroxyl oxygen of Tyr279 (of the M2-M3 loop) is hydrogen-bonded to the main-chain amino nitrogen of Leu142 (from the β 6- β 7 loop). The importance of the ECD-TMD interface is highlighted by the hyperekplexia mutations in GlyR α 1 clustered around the M2-M3 loop



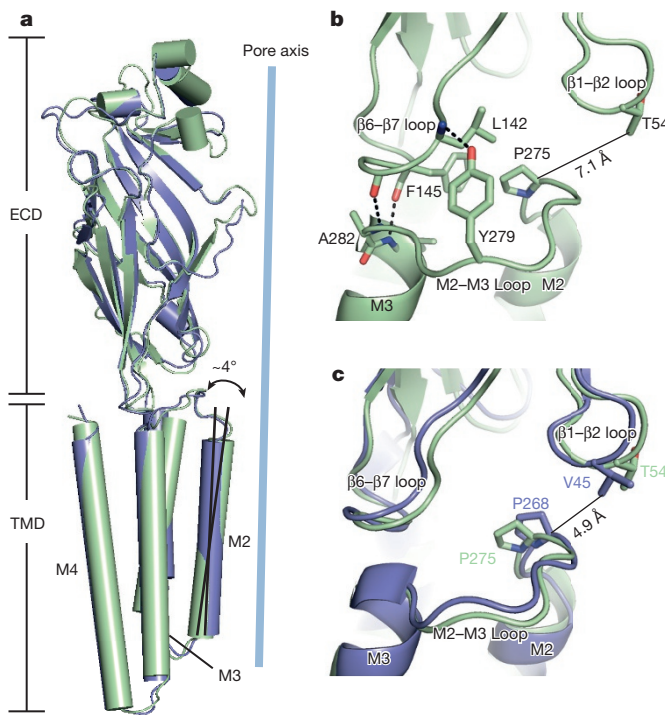


Figure 4 | Structural coupling at the ECD-TMD interface. **a**, Superposition of the ECDs of strychnine-bound GlyR α 3 (green) and apo-GluCl (blue) illustrates an \sim 4° tilt of the M2 pore-lining helix towards the pore axis. **b**, Illustration of key residues forming hydrogen bond and hydrophobic interactions that connect the ECD and TMD. Hydrogen bonds are denoted by dashed lines. The average distance from Pro275 C α to Thr54 C γ is noted. **c**, Superposition of the entire pentameric complex of strychnine-bound GlyR α 3 (green) and apo-GluCl (blue) reveals the position of the M2–M3 loop relative to the β1–β2 loop. The average distance from Pro268 C α to Val45 C γ in the apo-GluCl pentamer is noted.

(R271Q/L/P, K276E/Q, and Y279C/S) as they lead to reductions in glycine sensitivity and maximum probability of channel opening (Extended Data Fig. 5)¹².

All-atom molecular dynamics simulations of GluCl predicted that the unbinding of agonist at the orthosteric site and the opening of the orthosteric site lead to repositioning of the β1–β2 loop and inward displacement of the M2–M3 loop towards the pore, which is then coupled to the untilting of the M2 helix and the closing of the pore²⁹. This gating mechanism was subsequently validated by the apo-GluCl structure⁸ where the pore is closed, M2 helix is untilted from the pore by \sim 8°, and the M2–M3 loop shifts by more than 6 Å away from the channel pore, as visualized by the movement of Pro268 of the M2–M3 loop passing beneath Val45 on the β1–β2 loop. The M2–M3 loop of our strychnine-bound GlyR α 3 is much closer to the pore centre than in apo-GluCl structure (Fig. 4b). Pro275 of the M2–M3 loop is 7.1 Å from Thr54 of the β1–β2 loop in the strychnine-bound GlyR α 3 structure while the equivalent distance is 4.9 Å between Pro268 and Val45 in the apo-GluCl structure (Fig. 4c), suggesting that the M2–M3 loop in GlyR α 3 is pulled even more towards the pore than in apo-GluCl. Similar movement of the M2–M3 loop and the β1–β2 loop upon strychnine binding has also been observed in molecular dynamics simulations of a homology model of GlyR α 1 (ref. 30). This could lead to more energetic stabilization of the untilting of the M2 helix and the closing of the pore. Therefore, we hypothesize that the binding of the antagonist strychnine to GlyR α 3 induces the opening of loop C and the orthosteric binding pocket, which further facilitates the inward displacement of the M2–M3 loop and the tilting of the M2 helix towards the pore, ultimately leading to closing of the channel pore (Fig. 5).

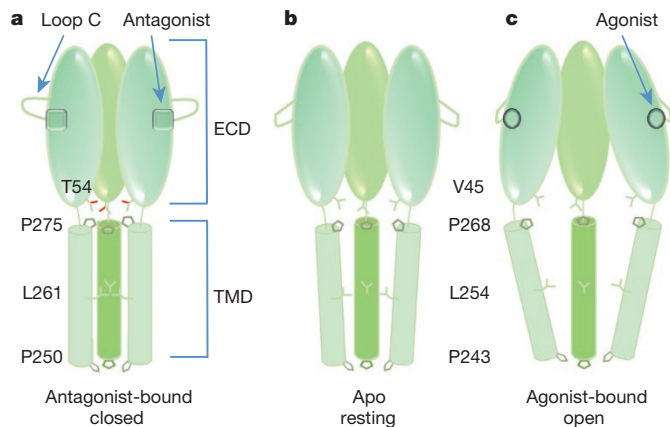


Figure 5 | Conformational changes in pLGICs. **a**, Schematic illustration of the conformation of the strychnine-bound closed GlyR α 3. **b**, Schematic illustration of the conformation of the apo resting GluCl. **c**, Schematic illustration of the conformation of the glutamate/ivermectin-bound open GluCl.

In summary, we present an X-ray structure of a GlyR, the human GlyR α 3 homopentamer, co-crystallized with the antagonist strychnine. Strychnine is bound in a larger orthosteric pocket and loop C of GlyR α 3 adopts an open conformation. The M2–M3 loop is displaced inwards, the pore-lining M2 helix tilts in a direction opposite to that observed in the active conformation of related pLGICs, and the pore is shut. Our study represents the first crystallographic analysis of a pLGIC in the inactive state induced by a competitive antagonist. These results shed new light on the conformational transitions upon antagonist binding and provide a rational basis for understanding human hyperekplexia mutations and the specificity of strychnine for GlyRs.

Online Content Methods, along with any additional Extended Data display items and Source Data, are available in the online version of the paper; references unique to these sections appear only in the online paper.

Received 1 April; accepted 23 July 2015.

Published online 28 September 2015.

1. Hilf, R. J. & Dutzler, R. X-ray structure of a prokaryotic pentameric ligand-gated ion channel. *Nature* **452**, 375–379 (2008).
2. Hilf, R. J. & Dutzler, R. Structure of a potentially open state of a proton-activated pentameric ligand-gated ion channel. *Nature* **457**, 115–118 (2009).
3. Bocquet, N. *et al.* X-ray structure of a pentameric ligand-gated ion channel in an apparently open conformation. *Nature* **457**, 111–114 (2009).
4. Sauguet, L. *et al.* Crystal structures of a pentameric ligand-gated ion channel provide a mechanism for activation. *Proc. Natl. Acad. Sci. USA* **111**, 966–971 (2014).
5. Hibbs, R. E. & Gouaux, E. Principles of activation and permeation in an anion-selective Cys-loop receptor. *Nature* **474**, 54–60 (2011).
6. Miller, P. S. & Aricescu, A. R. Crystal structure of a human GABA_A receptor. *Nature* **512**, 270–275 (2014).
7. Hassaine, G. *et al.* X-ray structure of the mouse serotonin 5-HT₃ receptor. *Nature* **512**, 276–281 (2014).
8. Althoff, T., Hibbs, R. E., Banerjee, S. & Gouaux, E. X-ray structures of GluCl in apo states reveal a gating mechanism of Cys-loop receptors. *Nature* **512**, 333–337 (2014).
9. Legendre, P. The glycinergic inhibitory synapse. *Cell. Mol. Life Sci.* **58**, 760–793 (2001).
10. Lynch, J. W. Molecular structure and function of the glycine receptor chloride channel. *Physiol. Rev.* **84**, 1051–1095 (2004).
11. Lynch, J. W. & Callister, R. J. Glycine receptors: a new therapeutic target in pain pathways. *Curr. Opin. Investig. Drugs* **7**, 48–53 (2006).
12. Bode, A. & Lynch, J. W. The impact of human hyperekplexia mutations on glycine receptor structure and function. *Mol. Brain* **7**, 2 (2014).
13. Schofield, P. R. *et al.* Sequence and functional expression of the GABA_A receptor shows a ligand-gated receptor super-family. *Nature* **328**, 221–227 (1987).
14. Langosch, D., Thomas, L. & Betz, H. Conserved quaternary structure of ligand-gated ion channels: the postsynaptic glycine receptor is a pentamer. *Proc. Natl. Acad. Sci. USA* **85**, 7394–7398 (1988).
15. Brejc, K. *et al.* Crystal structure of an ACh-binding protein reveals the ligand-binding domain of nicotinic receptors. *Nature* **411**, 269–276 (2001).

16. Celie, P. H. *et al.* Nicotine and carbamylcholine binding to nicotinic acetylcholine receptors as studied in AChBP crystal structures. *Neuron* **41**, 907–914 (2004).
17. Hansen, S. B. *et al.* Structures of *Aplysia* AChBP complexes with nicotinic agonists and antagonists reveal distinctive binding interfaces and conformations. *EMBO J.* **24**, 3635–3646 (2005).
18. Billen, B. *et al.* Molecular actions of smoking cessation drugs at $\alpha 4\beta 2$ nicotinic receptors defined in crystal structures of a homologous binding protein. *Proc. Natl Acad. Sci. USA* **109**, 9173–9178 (2012).
19. Moraga-Cid, G. *et al.* Allosteric and hyperekplexic mutant phenotypes investigated on an α_1 glycine receptor transmembrane structure. *Proc. Natl Acad. Sci. USA* **112**, 2865–2870 (2015).
20. Rajendra, S., Lynch, J. W. & Schofield, P. R. The glycine receptor. *Pharmacol. Ther.* **73**, 121–146 (1997).
21. Laube, B., Maksay, G., Schemm, R. & Betz, H. Modulation of glycine receptor function: a novel approach for therapeutic intervention at inhibitory synapses? *Trends Pharmacol. Sci.* **23**, 519–527 (2002).
22. Grenningloh, G. *et al.* Alpha subunit variants of the human glycine receptor: primary structures, functional expression and chromosomal localization of the corresponding genes. *EMBO J.* **9**, 771–776 (1990).
23. Jensen, A. A., Gharagozloo, P., Birdsall, N. J. & Zlotos, D. P. Pharmacological characterisation of strychnine and brucine analogues at glycine and $\alpha 7$ nicotinic acetylcholine receptors. *Eur. J. Pharmacol.* **539**, 27–33 (2006).
24. Mohsen, A. M., Heller, E., Holzgrabe, U., Jensen, A. A. & Zlotos, D. P. Structure–activity relationships of strychnine analogs at glycine receptors. *Chem. Biodivers.* **11**, 1256–1262 (2014).
25. Grudzinska, J. *et al.* The β subunit determines the ligand binding properties of synaptic glycine receptors. *Neuron* **45**, 727–739 (2005).
26. Brams, M. *et al.* A structural and mutagenic blueprint for molecular recognition of strychnine and *d*-tubocurarine by different Cys-loop receptors. *PLoS Biol.* **9**, e1001034 (2011).
27. Becker, C. M., Hoch, W. & Betz, H. Glycine receptor heterogeneity in rat spinal cord during postnatal development. *EMBO J.* **7**, 3717–3726 (1988).
28. Vandenberg, R. J., French, C. R., Barry, P. H., Shine, J. & Schofield, P. R. Antagonism of ligand-gated ion channel receptors: two domains of the glycine receptor α subunit form the strychnine-binding site. *Proc. Natl Acad. Sci. USA* **89**, 1765–1769 (1992).
29. Calimet, N. *et al.* A gating mechanism of pentameric ligand-gated ion channels. *Proc. Natl Acad. Sci. USA* **110**, E3987–E3996 (2013).
30. Yu, R. *et al.* Agonist and antagonist binding in human glycine receptors. *Biochemistry* **53**, 6041–6051 (2014).

Acknowledgements We thank G. Ranieri and R. Walter at Shamrock Structures and the staff at beamlines 08-ID at the Canadian Light Source and 22-ID at the Advanced Photon Source for data collection. We are grateful to Z. Wang and J. Gingras for reviewing the manuscript.

Author Contributions The authors have jointly contributed to project design, data analysis and manuscript preparation. P.L.S. performed initial construct design and purification experiments, structure solution, model building, and structural analysis; X.H. performed protein purifications, crystallization, model building, and structural analysis; H.C. performed cloning and expression experiments; K.M. performed SPR and ITC binding studies; S.S. performed functional testing; P.L.S. and X.H. wrote the manuscript with help from K.M., S.S., and H.C.

Author Information Atomic coordinates and structure factors for the GlyR $\alpha 3$ –strychnine complex have been deposited in the Protein Data Bank (PDB) under accession number 5CFB. Reprints and permissions information is available at www.nature.com/reprints. The authors declare no competing financial interests. Readers are welcome to comment on the online version of the paper. Correspondence and requests for materials should be addressed to X.H. (hxin@amgen.com) or P.L.S. (pshaffer@amgen.com).

METHODS

No statistical methods were used to predetermine sample size. The experiments were not randomized. The investigators were not blinded to allocation during experiments and outcome assessment.

GlyR α 3 construct, expression, and purification. The GlyR α 3_{cryst} protein construct was derived by removal of the M3–M4 loop on the basis of alignments with bacterial channels and the *C. elegans* GluCl α crystallization construct and replaced with a tri-peptide linker (AGT). The C terminus was truncated by four residues on the basis of sequence alignments with various mammalian GlyR α 3 sequences. To facilitate purification, a Strep II affinity tag (WSHPQFEK) was added to the C terminus. In total, GlyR α 3_{cryst} corresponds to the polypeptide sequence of human GlyR α 3 (Uniprot O75311) 1–460 (Δ 343–418::AGT)-Strep. The recombinant baculovirus was generated with the Bac-to-Bac system (Life Technologies). Expression was done by baculovirus transduction of Sf9 insect cells grown in sf9 medium (Hyclone) at 27 °C for 72 h. Cells were harvested by centrifugation at 2,000g and disrupted in an Microfluidizer in a buffer containing 50 mM Tris pH 8.0, 150 mM NaCl, and 1% protease inhibitors cocktail (Sigma). The homogenate was clarified by centrifugation at 10,000g and crude membranes were collected by centrifugation at 125,000g. The membrane were mechanically homogenized and solubilized in 0.2 g DDM per gram of membranes in 20 mM Tris pH 8.0, 150 mM NaCl, 0.5% protease inhibitors cocktail. Solubilized membranes were centrifuged at 125,000g and supernatant was bound to Strep affinity resin (IBA), washed with 20 mM Tris pH 8.0, 150 mM NaCl, 1 mM DDM, and eluted with 20 mM Tris pH 8.0, 150 mM NaCl, 1 mM DDM, and 5 mM desthiobiotin. Eluted fractions containing GlyR α 3_{cryst} were pooled together, concentrated, and further purified by gel filtration in 20 mM Tris pH 8.0, 150 mM NaCl, and 1 mM DDM. All purification steps were performed at 4 °C.

Crystallization and data collection. Purified GlyR α 3 were concentrated to ~3 mg ml⁻¹ and incubated with 0.2 mM strychnine at 4 °C for 30 min before crystallization. Crystals of GlyR α 3–strychnine were obtained in hanging drop at 4 °C by mixing 0.5 µl of the GlyR α 3–strychnine complex with 0.5 µl of the crystallization buffer containing 25 mM sodium citrate pH 4.0, 100 mM KCl, 200 mM MgCl₂, 30–33% PEG400. Crystals take about 1 month to grow and were frozen directly from the crystallization drops in liquid nitrogen for data collection. Diffraction data were collected at beamline 22-ID at the Advanced Photon Source, Argonne National Laboratory. Diffraction data were indexed, integrated, and scaled using HKL2000 software³¹. Despite screening many crystals at the synchrotron, the highest resolution data set obtained from a single crystal was 3.5 Å owing to their relatively small size and rapid degradation upon exposure to high-intensity X-ray beams. The final complete 3.0 Å data set was assembled by merging data from 15 separate crystals with 10–30° of data collected from each crystal to limit radiation damage (Extended Data Table 1).

Structure determination. Initial phases for the structure were generated by molecular replacement with Phaser³² using the pentameric apo-GluCl structure as a search model (PDB accession number 4TNV)⁸. A clear solution was obtained with one pentameric assembly of GlyR α 3 in the asymmetric unit. Electron density maps were improved by fivefold non-crystallographic symmetry averaging. Initial maps were of sufficient quality to build strychnine molecules and GlyR α 3 side chains where they differed from those of GluCl. In agreement with established conventions, the residue numbering scheme reassigns residue Ala34 of the Uniprot sequence as Ala1 because it is the first amino acid in the mature polypeptide following removal of the secretion signal sequence. Additionally, residue numbering in the GlyR α 3_{cryst} model is continuous, meaning residues following the deletion of the intracellular domain between M3 and M4 do not retain their numbering from the wild-type protein. The restraint parameters for strychnine were generated by PRODRG³³. Iterative rounds of restrained refinement in Refmac5³⁴ and manual rebuilding in Coot³⁵ were used to improve the model. In final rounds of refinement, fivefold non-crystallographic symmetry restraints were removed and ten TLS parameters added, one each for the ECD and the TMD of the five protomers in the structure. Model quality was assessed using Molprobity³⁶. The final model consists of one GlyR α 3 pentamer including residues 9–347, N-linked glycosylation at Asn38, and five strychnine molecules (Extended Data Table 1). Electrostatic surface potential calculations were performed using the APBS³⁷ Tool plug-in in PyMOL and pore dimensions were analysed with HOLE³⁸. Images were made using PyMOL³⁹. Sequence alignment was performed in ClustalW⁴⁰.

ITC and SPR binding experiments. ITC experiments were performed on an ITC200 instrument (GE Healthcare). Protein concentration was determined by absorbance at 280 nm using a molar extinction coefficient per cm of 66,600. For titration experiments, GlyR α 3 was diluted to 7 µM in phosphate buffered saline (PBS) pH 7.4 and placed in the ITC cell. Freshly prepared strychnine (10 mM stock in dimethylsulfoxide (DMSO)) was diluted to 100 µM in PBS pH 7.4 and placed in the syringe. Final DMSO concentration in the cell and syringe was 1% (v/v).

Strychnine titration into buffer was also performed to ensure minimal heat of dilution. Titrations were performed at 25 °C using 2 µl injections (4 s duration, 180 s spacing, and 5 s filter period). Reference power was set to 10 µcal s⁻¹ and stirring speed to 1,000 r.p.m. The raw data were baseline corrected and integrated using Origin 7.0. All thermodynamic parameters were obtained from the fitting of the heat data assuming 1:1 interaction model. Binding experiments were performed twice ($n = 2$) to calculate a standard deviation.

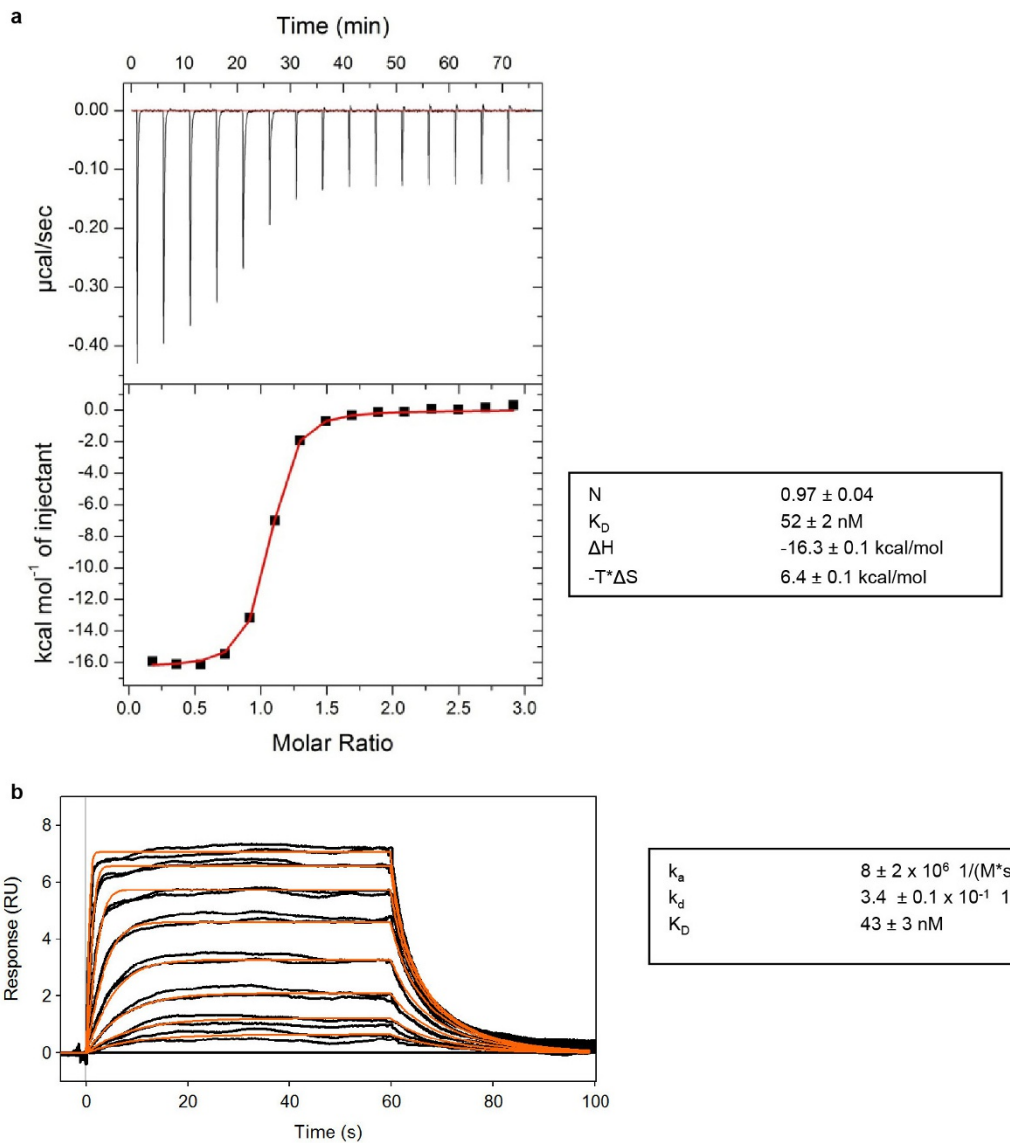
SPR measurements were performed on a Biacore T200 (GE Healthcare) at 25 °C using PBS pH 7.4 as running buffer. L1 chips were pre-conditioned with three 30 s injections of 20 mM CHAPS. GlyR α 3 was diluted to 300 µg ml⁻¹ in PBS pH 7.4 containing 1 mM DDM and 0.1 mg ml⁻¹ POPG. GlyR α 3 was passed over L1 chip and captured onto the biosensor at a density of 4,000 response units. In the reference cell, solution with lipid (that is, no GlyR α 3) was injected. DMSO at 1% (v/v) was added to the running buffer and strychnine injected at various concentrations (top concentration 2 µM, twofold dilution series, in duplicate) at a flow rate of 90 µg min⁻¹. The association was set to 1 min followed by 2 min dissociation. The raw data were processed using Scrubber2 software (BioLogic Software) and the data kinetically fitted to a 1:1 binding model which included a mass transfer limitation term. Binding experiments were performed three times ($n = 3$) to calculate a standard deviation.

Functional testing in FLIPR assay⁴¹. HEK293T cells were cultured in Cell Culture Media (MEM supplemented with 10% v/v qualified heat-inactivated FBS, 100 units penicillin, 100 units streptomycin, 29.2 mg ml⁻¹ of L-glutamine) under standard cell culture conditions of 37 °C, 5% v/v CO₂, and 95% humidity. Cells were grown in T 225 cm² culture flasks to a density of approximately 8×10^7 cells and harvested after about 4 days by briefly washing with DPBS followed by addition of Cell Dissociation Reagent for 2 min. The concentration of cells in suspension was adjusted to 6.40×10^5 cells per millilitre in Cell Plating Media (MEM with 10% dialysed FBS, 100 units penicillin, 100 units streptomycin, 0.29 mg ml⁻¹ of L-glutamine and 10 mM HEPES pH 7.4) and transduced with either wild-type GlyR α 3 (MOI = 1) or GlyR α 3_{cryst} (MOI = 5) baculovirus containing a BacMam vector with a CMV promoter. Using a Multidrop Combi, 25 µl of cell suspension was dispensed into Corning CellBIND 384-well ViewPlates. Transduced cell culture plates were then incubated at 37 °C overnight under the standard cell-culture conditions described above. The next day (about 18–24 h after plating), 5 µl of 6× Membrane Potential blue dye for monitoring changes in membrane potential was dispensed into each cell culture plate using a Thermo Multidrop Combi (prepared in assay buffer at 6× the manufacturer's recommended final concentration). The cell plates were then incubated at 37 °C for 30 min and allowed to equilibrate to room temperature (25 °C) for an additional 30 min.

Glycine dose-response plates were prepared in assay buffer (10 mM HEPES, 60 mM NaCl, 5 mM KCl, 2 mM MgCl₂, 1 mM CaCl₂, 10 mM D-glucose, 160 mM D-mannitol and 2 M KOH solution to adjust pH to 7.4) supplemented with 2% v/v DMSO using a 1:2 stepwise dilution series in standard 384-well polypropylene plates. The membrane potential assay is performed on FLIPR Tetra, which transfers 10 µl from the 4× glycine dose-response plate and adds it to the 30 µl volume in each well of the cell plate containing Membrane Potential blue dye. Fluorescence emission (510–545 nm/565–625 nm excitation/emission filter set, excitation intensity 40%, camera gain 50, and an exposure time of 0.4 s) is measured in real-time to detect changes in membrane potential. The net membrane potential of the cells changes upon activation of GlyR α 3, which results in the increased flux of chloride ions out of the cell down a concentration gradient and a robust increase in fluorescence signal. FLIPR kinetic traces were processed using an area under the curve relative to baseline algorithm, where the baseline was the first 10 s of the measurement before addition of glycine to the cell plate. All measurements proceeded for 120 s post-addition. The processed data were subsequently normalized to the maximum achievable glycine response (at 2 mM glycine). Normalized data were then plotted against log[glycine] and data were fitted to a nonlinear regression four-parameter Hill fit to determine the half-maximum effective concentration/half-maximum inhibitory concentration (EC₅₀/IC₅₀) from the resulting sigmoidal curve. All curve fitting was performed with GraphPad Prism 6 software.

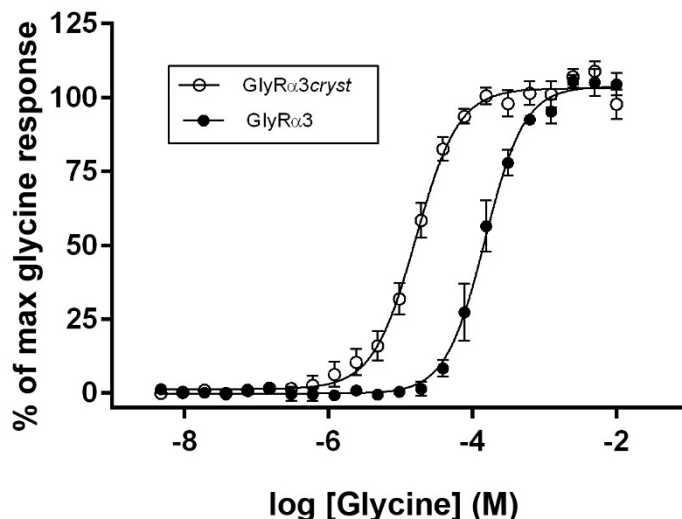
31. Otwinowski, Z. & Minor, W. Processing of X-ray diffraction data collected in oscillation mode. *Methods Enzymol.* **276**, 307–326 (1997).
32. McCoy, A. J. Solving structures of protein complexes by molecular replacement with Phaser. *Acta Crystallogr. D* **63**, 32–41 (2007).
33. Schuttelkopf, A. W. & van Aalten, D. M. PRODRG: a tool for high-throughput crystallography of protein-ligand complexes. *Acta Crystallogr. D* **60**, 1355–1363 (2004).
34. Murshudov, G. N., Vagin, A. A. & Dodson, E. J. Refinement of macromolecular structures by the maximum-likelihood method. *Acta Crystallogr. D* **53**, 240–255 (1997).
35. Emsley, P. & Cowtan, K. Coot: model-building tools for molecular graphics. *Acta Crystallogr. D* **60**, 2126–2132 (2004).
36. Davis, I. W. et al. MolProbity: all-atom contacts and structure validation for proteins and nucleic acids. *Nucleic Acids Res.* **35**, W375–W383 (2007).

37. Baker, N. A., Sept, D., Joseph, S., Holst, M. J. & McCammon, J. A. Electrostatics of nanosystems: application to microtubules and the ribosome. *Proc. Natl Acad. Sci. USA* **98**, 10037–10041 (2001).
38. Smart, O. S., Neduvelli, J. G., Wang, X., Wallace, B. A. & Sansom, M. S. HOLE: a program for the analysis of the pore dimensions of ion channel structural models. *J. Mol. Graph.* **14**, 354–360, 376 (1996).
39. DeLano, W. L. The PyMOL molecular graphics system (DeLano Scientific, 2002).
40. Larkin, M. A. et al. Clustal W and Clustal X version 2.0. *Bioinformatics* **23**, 2947–2948 (2007).
41. Jensen, A. A. & Kristiansen, U. Functional characterisation of the human $\alpha 1$ glycine receptor in a fluorescence-based membrane potential assay. *Biochem. Pharmacol.* **61**, 1789–1799 (2004).



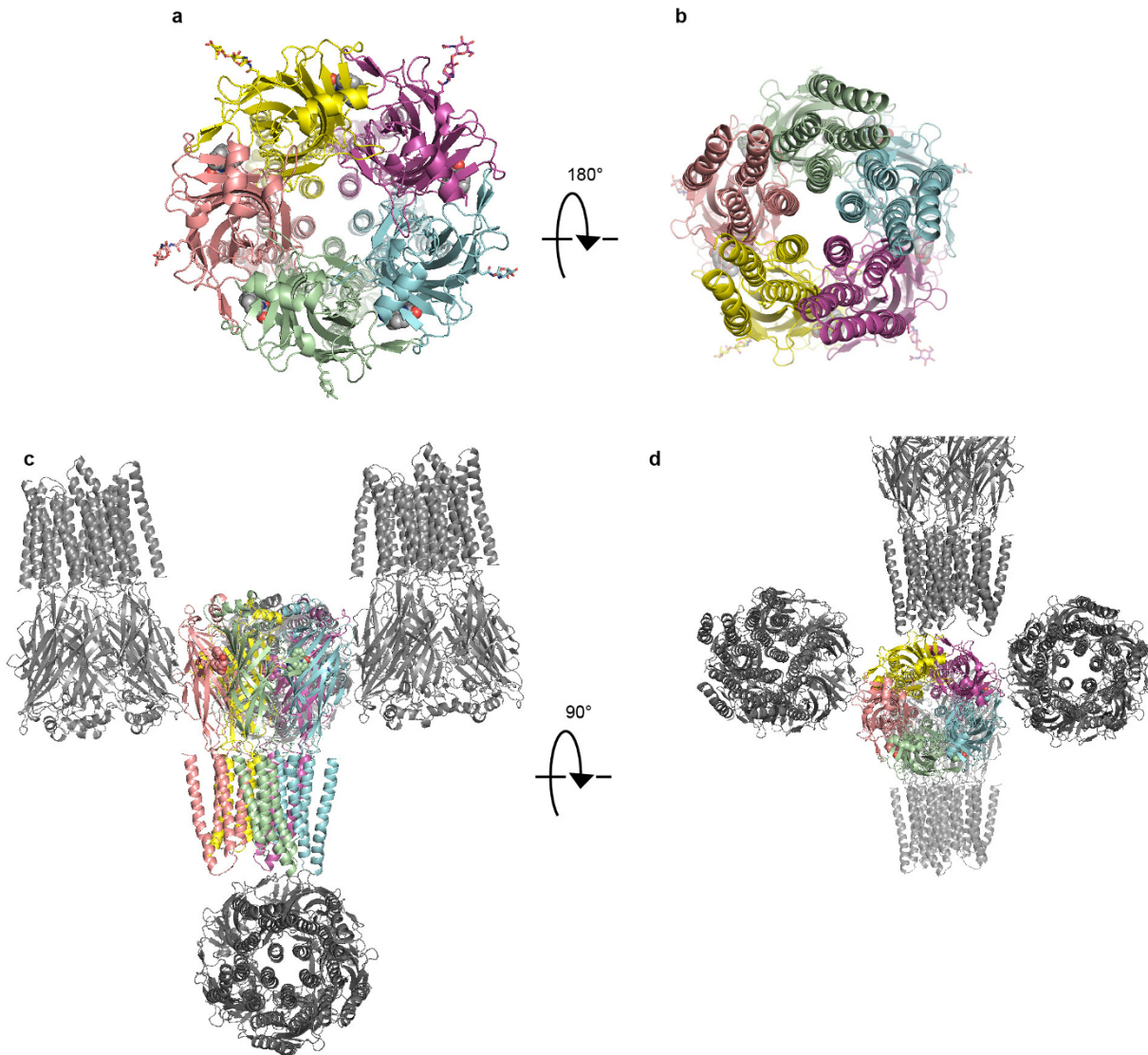
Extended Data Figure 1 | Strychnine binding to GlyR $\alpha 3_{\text{cryst}}$ in detergent micelles. **a**, Binding thermodynamics and stoichiometry of strychnine to GlyR $\alpha 3_{\text{cryst}}$ analysed by ITC. The individual peaks from titrations are integrated and presented in a Wiseman plot. An appropriate binding model is

chosen and the isotherm is then fitted to yield the binding enthalpy ΔH , the dissociation constant K_D , and the stoichiometry n . **b**, Binding kinetics of strychnine to GlyR $\alpha 3_{\text{cryst}}$ measured by SPR spectroscopy.



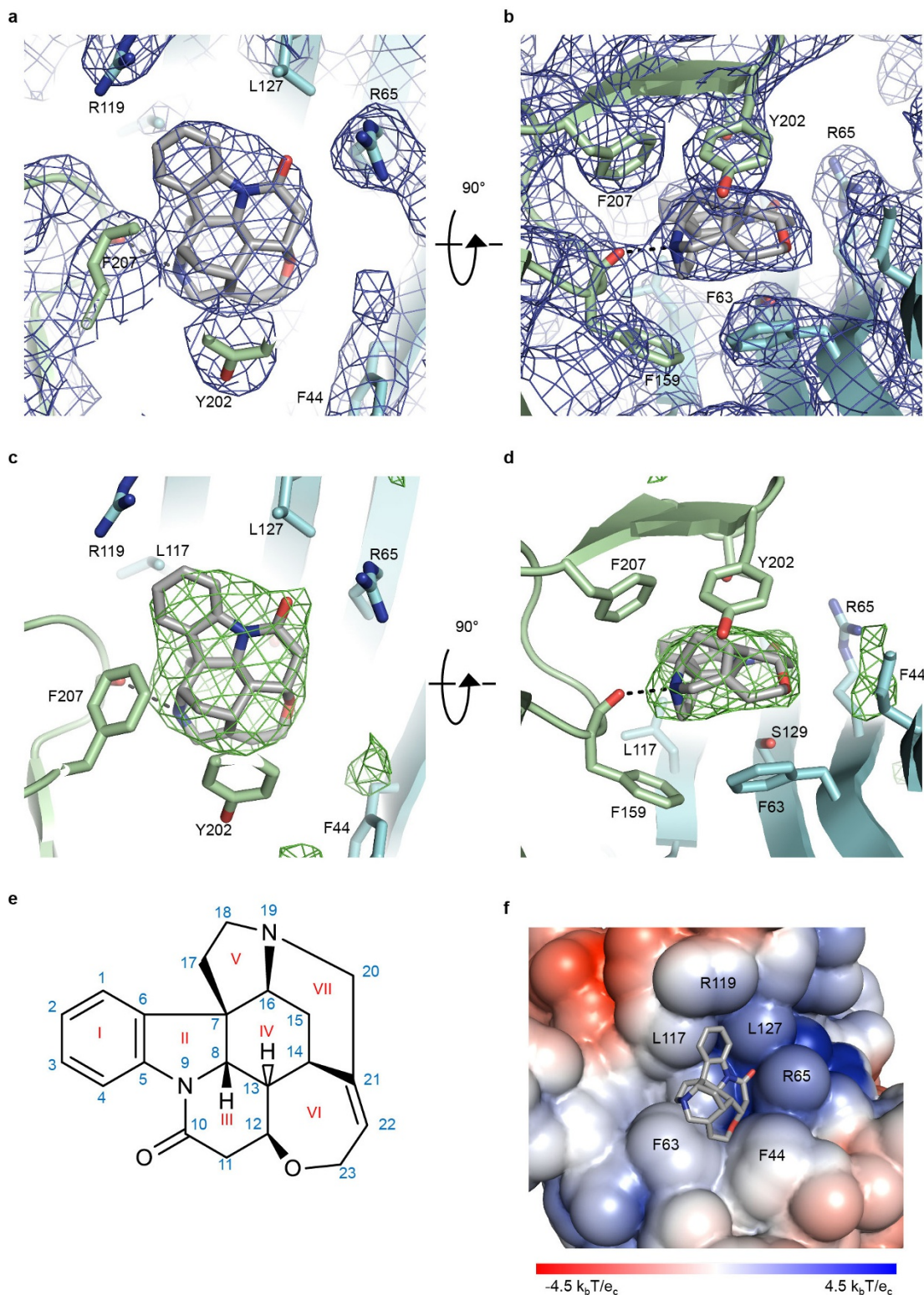
Extended Data Figure 2 | Glycine dose–response to GlyR α 3_{cryst} in HEK293T cells. Glycine dose–response curve for BacMam baculovirus-transduced HEK293T cells expressing either wild-type human GlyR α 3 (GlyR α 3, filled circles) or GlyR α 3_{cryst} (open circles) measured by membrane potential dye assay (see Methods for details). Each data point represents a value

of $n = 4\text{--}6$ and normalized to a maximum glycine response observed at 2 mM glycine concentration. Glycine EC₅₀ for GlyR α 3 was calculated at $150 \pm 10.6 \mu\text{M}$ ($n = 4$, 95% confidence interval) and GlyR α 3_{cryst} at $16.4 \pm 1.2 \mu\text{M}$ ($n = 5$, 95% confidence interval).



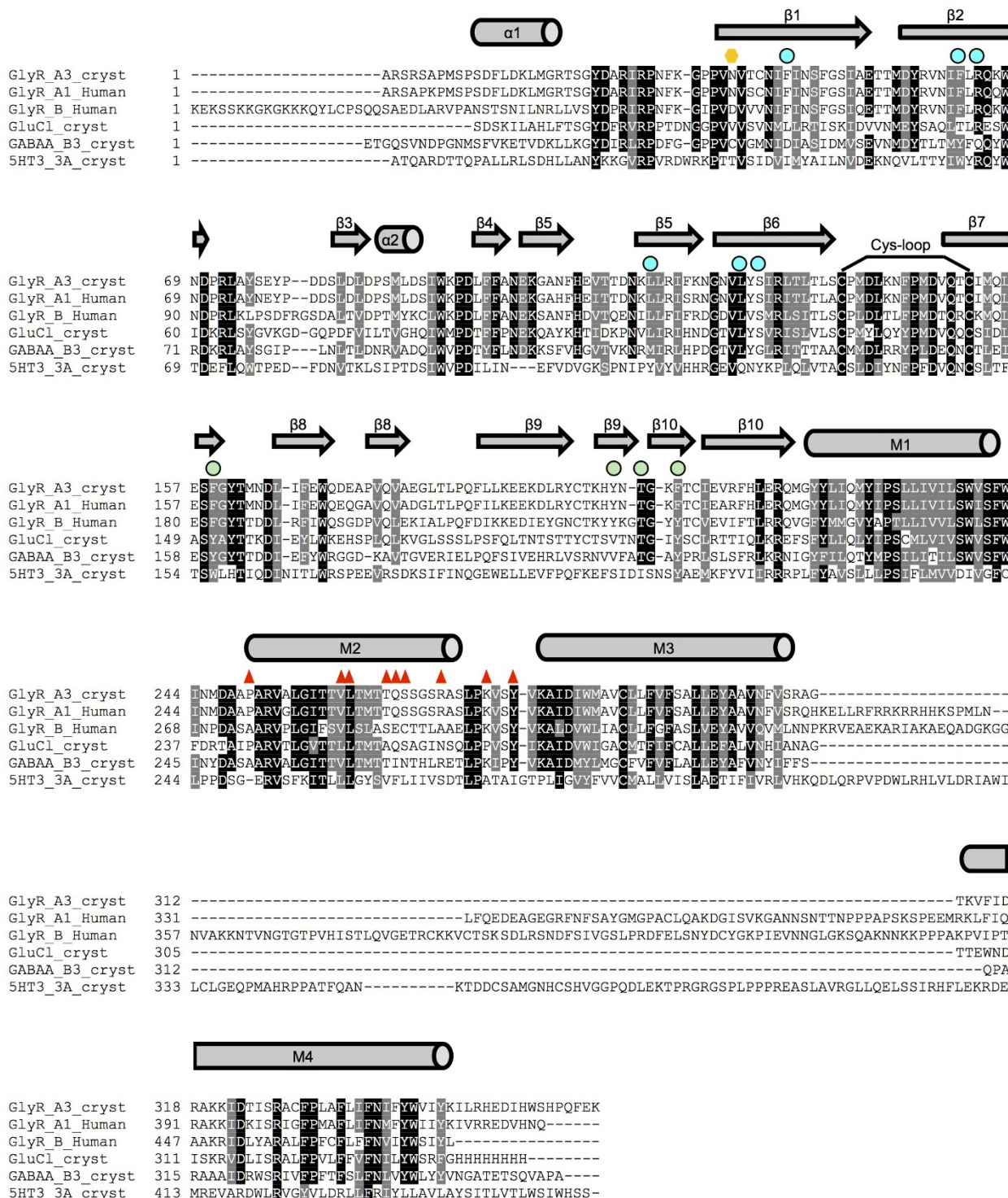
Extended Data Figure 3 | Architecture of the GlyR α 3 bound to strychnine and crystallographic packing of GlyR α 3_{cryst}. **a**, The GlyR α 3–strychnine complex viewed from the extracellular side of the membrane down the pore axis, perpendicular to the membrane. Strychnine is bound at the interface between subunits. **b**, The GlyR α 3–strychnine complex viewed from the intracellular side down the pore axis. The M2 helices are shown lining the pore. **c, d**, Packing of the GlyR α 3–strychnine complex. Receptor in the asymmetric

unit is coloured by subunit, with subunit A in pale green and subunit B in cyan. Strychnine molecules are shown as spheres and are coloured to match their associated principal subunit. Symmetry-related receptors are coloured grey. The interface between subunits A and B is completely exposed to solvent in the crystal lattice, and this interface was used in the making of all figures for this paper to avoid any potential crystal-packing artefacts.



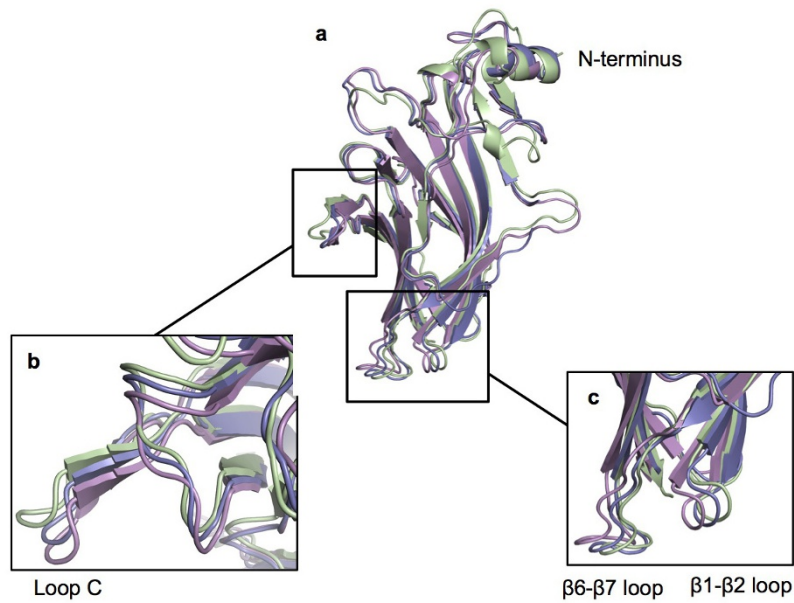
Extended Data Figure 4 | Strychnine binding to GlyR α 3. **a, b,** Two views of the strychnine-binding pocket showing $2F_o - F_c$ omit electron density maps. The principal subunit is coloured pale green, the complementary subunit is cyan, and strychnine is grey. Strychnine was omitted from map calculations. Map is contoured at 1.0σ . The hydrogen bond between the backbone carbonyl of Phe159 and the tertiary nitrogen of strychnine is shown as a dotted line. **c, d,** Same views and representations as in **a** and **b**, but $F_o - F_c$ omit electron

density is shown. Contour level of map is 3.0σ . **e,** Chemical structure of strychnine. Ring numbering is denoted by red Roman numerals. Carbon and nitrogen historic numbering conventions are denoted by blue numbers. **f,** Solvent-accessible surface area of the complementary side of the binding interface coloured by electrostatic potential. The complementary subunit interface has a positive electrostatic potential to interact with the partial negative charge of the lactam oxygen of strychnine.



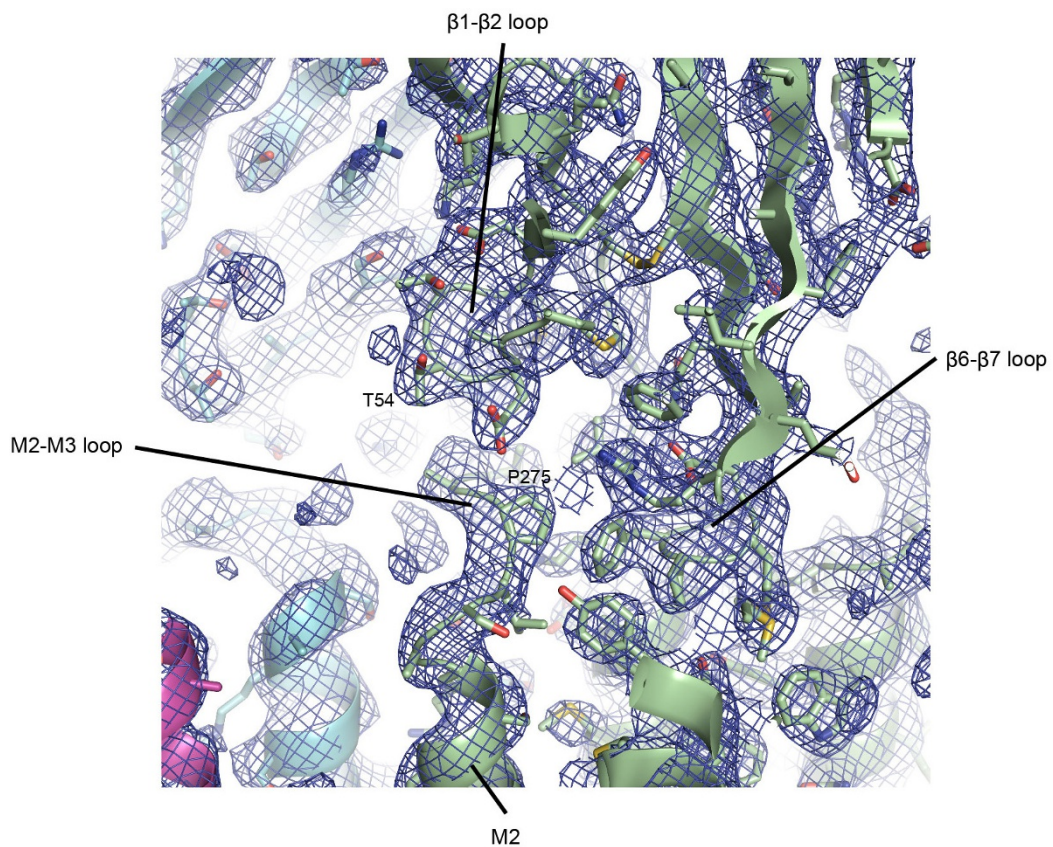
Extended Data Figure 5 | Sequence alignment of GlyR α 3_{cryst} with representative eukaryotic Cys-loop receptor family members. Residue conservation is indicated by grey and black highlights. Site of N-linked glycosylation of GlyR α 3_{cryst} is indicated by the orange hexagon. Residues involved in binding of strychnine are indicated by green (the principal subunit) and cyan (the complementary subunit) dots. Red triangles above residues indicate mutations in GlyR α 1 or GlyR β that cause hyperekplexia. Signal peptides have been removed from all protein sequences. Secondary structure elements are denoted by cylinders (helices) and arrows (strands) above the alignment. The alignment was generated using ClustalW. Protein sequences are from the following entries: human GlyR α 1 (Uniprot P23415), human GlyR β (Uniprot 48167), GluCl_{cryst} (PDB accession number 4TNV), GABA A R- β 3_{cryst} (PDB accession number 4COF), and 5HT $3A$ (PDB accession number 4PIR).

peptides have been removed from all protein sequences. Secondary structure elements are denoted by cylinders (helices) and arrows (strands) above the alignment. The alignment was generated using ClustalW. Protein sequences are from the following entries: human GlyR α 1 (Uniprot P23415), human GlyR β (Uniprot 48167), GluCl_{cryst} (PDB accession number 4TNV), GABA A R- β 3_{cryst} (PDB accession number 4COF), and 5HT $3A$ (PDB accession number 4PIR).



Reference	Moving	C α Positions	RMSD (Å)
GlyR α 3 Pentamer (A-E/*)	GluCl-apo (4TNV)	1586	1.76
"	GluCl-POPC (4TNW)	1615	1.79
"	GluCl-Ivermectin (3RIF)	1586	2.39
"	GABA A_R -β3 (4COF)	1456	3.11
GlyR α 3 ECD Monomer (A/9-219)	GluCl-apo (4TNV)	193	1.19
"	GluCl-POPC (4TNW)	201	1.13
"	GluCl-Ivermectin (3RIF)	200	1.28
"	GABA A_R -β3 (4COF)	203	1.38
GlyR α 3 TMD Pentamer (A-E/220-247)	GluCl-apo (4TNV)	619	1.42
"	GluCl-POPC (4TNW)	619	2.47
"	GluCl-Ivermectin (3RIF)	592	2.72
"	GABA A_R -β3 (4COF)	514	3.40

Extended Data Figure 6 | Structural alignment of pLGICs. **a**, Structures of GlyR α 3_{cryst} (green), apo-GluCl α (slate), and glutamate- and ivermectin-bound GluCl α (violet) aligned using their ECDs. **b**, Close-up view of the loop C, rotated 45° clockwise along the horizontal axis (left to right) to optimize viewing. **c**, Close-up view of loops β6-β7 and β1-β2. **d**, Table showing regions of GlyR α 3 used for structural alignments, as well as resulting number of overlapped C α atoms and root mean squared deviation distances. PDB accession numbers are listed for each reference structure.



Extended Data Figure 7 | Representative electron density for the ECD–TMD interface. Final $2F_o - F_c$ electron density map around the region of the ECD–TMD interface is shown, contoured at 1.0σ . Protomer A is shown in pale green, protomer B in cyan, and protomer C in magenta. Important secondary structure elements and loops are noted.

Extended Data Table 1 | Crystallographic and structure refinement statistics

GlyR α 3 _{cryst} + strychnine	
Data collection	
Space group	P2 ₁ 2 ₁ 2 ₁
Cell dimensions	
<i>a</i> , <i>b</i> , <i>c</i> (Å)	140.2, 140.2, 180.1
α , β , γ (°)	90.0, 90.0, 90.0
Resolution (Å)	50-3.04 (3.15-3.04) *
<i>R</i> _{merge}	0.209 (1.177)
<i>R</i> _{pim}	0.064 (0.452)
<i>I</i> / σ <i>I</i>	8.5 (1.3)
Completeness (%)	96.9 (77.6)
Redundancy	10.1 (5.8)
CC _{1/2}	0.983 (0.573)
Refinement	
Resolution (Å)	50-3.04
No. reflections	67970
<i>R</i> _{work} / <i>R</i> _{free}	0.243/0.258
No. atoms	
Protein	13317
Ligand/ion	223
Water	0
B-factors	
Protein	124
Ligand/ion	120
R.m.s deviations	
Bond lengths (Å)	0.006
Bond angles (°)	1.05

This structure was determined from fifteen crystals.

*Highest resolution shell is shown in parenthesis.